Measurements and analysis of neutron elastic scattering at 65 MeV

E. L. Hjort,* F. P. Brady, J. L. Romero, J. R. Drummond,
D. S. Sorenson,† J. H. Osborne, and B. McEachern
Crocker Nuclear Laboratory and Department of Physics, University of California, Davis, California 94550

L. F. Hansen
Lawrence Livermore National Laboratory, Livermore, California 94550
(Received 7 March 1994)

Elastic scattering cross sections for 65 MeV neutrons have been measured for natural targets of C, Si, Cd, Fe, Sn, and Pb at laboratory angles from 6° to 45°. A unique, compact detection system consisting of a CH_2 (proton) converter and large-acceptance, wire-chamber-based, recoil-proton telescope is utilized for the measurements. The data are compared with macroscopic optical model potentials derived from proton scattering. In addition, comparisons with the microscopic optical model potentials, those of Jeukenne-Lejeune-Mahaux and Yamaguchi-Nagata-Matsuda, give a very good fit to the data.

PACS number(s): 25.40.Dn, 24.10.Ht

I. INTRODUCTION

Measurements of neutron elastic scattering at 65 MeV are presented for natural targets of C, Si, Ca, Fe, Sn, and Pb from 6° to 45°. The present work extends the energy range of the few measurements done at 30 and 40 MeV at Michigan State University (MSU) [1–3] in the early eighties. The study of the energy dependence of effective interactions in microscopic optical model potentials, the dependence of the imaginary potential in the phenomenological model, Coulomb effects, and charge symmetry are [4] some of the theoretical motivations for neutron scattering measurements at higher energies.

Phenomenological optical model potentials (OMP's) have been used extensively in the analysis of neutron scattering data at lower energies, and reasonably good fits to the data have been obtained by using global optical model parameter sets which have a well behaved dependence on the incident energy (E) and the A and Z values of the target nucleus. Improvements in the fits to the data can be obtained with parameters that deviate from those prescribed by the global sets. However, higher-resolution nucleon scattering data available at lower energies ($\leq$ 25 MeV) have shown the limitations of the phenomenological OMP's. Hodgson [5] in his review of the phenomenological optical potential has discussed the need for further parametrization of the potentials in order to reproduce the fine structure observed in proton scattering data and high-resolution neutron total cross sections.

Microscopic [6–8] OMP's have been tested [9–12] extensively against a large body of proton and neutron elastic scattering and analyzing power data in the last ten years and over a wide range of incident energies below 30 MeV and mass numbers between Li and Pb. These potentials are described by a one-step folding model of an effective two-body interaction derived from a free nucleon-nucleon potential and the nuclear density. Quite good agreement with the measurements has been obtained with no more than two or three parameters which show a smooth dependence on energy (E) and mass number (A).

In the present work, the measured neutron angular distributions at 65 MeV are compared to calculations with phenomenological and microscopic OMP's. The macroscopic optical potentials of Watson, Singh, and Segel [13], Becchetti-Greenlees [14], Comfort-Karp [15], Schwandt *et al.* [16], and Schutt *et al.* [17] were used in the phenomenological OMP calculations. The microscopic optical model calculations were done for the potentials of Jeukenne-Lejeune-Mahaux [7] and Yamaguchi-Nagata-Matsuda [8]. The quality of the agreement with the data for the phenomenological and microscopic OMP's is discussed in the paper.

II. EXPERIMENT

The 65 MeV elastic neutron data were measured using the compact detection system [18] at Crocker Nuclear Laboratory on the campus of the University of California at Davis. The system [18] (Fig. 1) was originally developed for $(n, n'x)$ measurements. For the latter, time of flight is difficult to use, because elastic scattering of the lower-energy tail (or continuum) of the neutron beam spectrum falls in the same energies as the $(n, n'x)$ continuum. The neutron beam is produced by ^{7}Li$(p, n)^7$Be and collimated by 1.5 m of steel. It has a resolution of

*Present address: Physics Department, Purdue University, West Lafayette, IN 47907.
†Present address: P15, Los Alamos National Laboratory, Los Alamos, NM 87545.

 ©1994 The American Physical Society

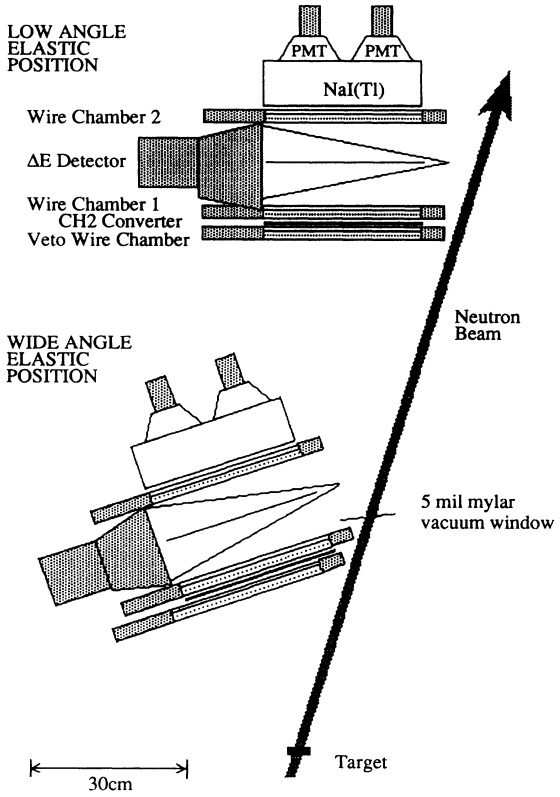

FIG. 1. Scale drawing of the two geometries used for measurement of elastic scattering cross sections. For the low-angle measurements the beam was in vacuum up to the 5 mil Mylar window shown in figure.

$\approx$ 1.2 MeV full width at half maximum (FWHM), due largely to the thickness of the ^{7}Li target used, and a flux of $\simeq 10^6$ neutrons/sec. The system utilizes multiwire chambers to track recoil protons which result from n-p conversions of the scattered neutrons in a large-area (30×30 cm^2) CH_2 converter. The energy of the scattered neutron is found from the angle of the n-p conversion and from the energy of the recoil proton as measured in a large-area (30×15 cm^2) NaI(Tl) detector. (Nonrelativistically, $E_p = E_n \cos^2 \theta_{np}$.) The overall resolution of the spectra (2.7 MeV) is a result of the combined effects from the neutron beam's resolution, energy losses in the converter, the resolution of the NaI(Tl) detector, and uncertainties in the proton's recoil angle. The last is due primarily to the size (adjustable by collimator inserts,but usually 2×4 cm^2 or 2×2 cm^2) of the target beam spot and target-detector distance. The predicted resolution is 2.4 MeV as expected from nearly equal contributions from the above four effects [18,19]. The resolution difference is attributed largely to uncertainties in the response map of the E detector which is an important factor in the energy resolution. As shown in Fig. 1, two detector geometries were used to measure scattering angles of 6° to 48° in the lab frame. The wide-angle geometry with the CH_2 converter at 35 cm from the target measured angles greater than 18° with an angular resolution of $\pm 1.5°$ due to the size of the beam spot on the target. The low-angle geometry with the converter at $\simeq$ 1 m measured angles of less than 20° with an improved resolution of better than $\pm 1.0°$ due to its increased distance from the target. The "veto" chamber in front of the converter was used to veto charged particles.

The targets were fairly thick, having a fractional interaction probability in the range $\simeq$ 15–21 %, except for Si which was calculated to be 25% and measured to be 27% (using the beam attenuation method). The neutron beam is monitored using a recoil-proton telescope at $\approx$ 8 m from the ^{7}Li target, with the integrated charge of the proton beam deflected into a Faraday cup serving as a secondary monitor.

In the data analysis, time-of-flight (TOF) cuts are used to delineate and separate neutron beam peak from beam tail events. Cuts on ΔE vs E spectra allow separation of protons from deuterons and tritons. The latter are produced by $C(n,d)$ and (n,t) reactions in the CH_2 converter.

Figure 2 shows some extracted neutron energy spectra. The energy dependence of the (more convenient) Binstock n-p parametrization [20] was used in the conversion of proton to neutron spectra. This parametrization [20] was used in the conversion of proton to neutron spectra. This parametrization differs by $\leq 3\%$ from values based on the more recent Arndt phases [21], which are used to provide absolute cross section normalization.

The data were corrected for nuclear interactions in the NaI, for the effects of attenuation and multiple scattering in the target, for the angular resolution of the system, and for those low-lying excited states which were not resolved from the elastic peak. For the last correction, (p,p') cross sections were used to provide strengths of the low-lying states and DWUCK4 was used to convert these to (predicted) (n,n') cross sections. Typically the net correction applied to a given data point was a few percent or less, although for a few points the correction was at the 10% level. Data were also taken with no target to measure the background, which in all cases was minimal. More details are given by Hjort [22].

A CH_2 target was used to observe ^{1}H$(n,n)^1$H scattering (Fig. 2) for normalization purposes. Except at forward angles the ^{1}H$(n,n)^1$H peaks are kinematically separated in energy from the ^{12}C$(n,n)^{12}$C peaks. In any case, data taken with a C target were subtracted from the CH_2 spectra, yielding the ^{1}H$(n,n)^1$H spectra. The cross section for ^{1}H$(n,n)^1$H at 65 MeV obtained from Ref. [21] was used to normalize the data from the other targets. The normalization process involved the relative beam flux and thickness for each target. The effects of varying beam attenuations in the different targets were also taken into account.

III. MEASUREMENTS AND OPTICAL MODEL ANALYSES

Phenomenological OMP's

Measured elastic scattering (c.m.) cross sections are shown in Fig. 3 together with the calculations us-

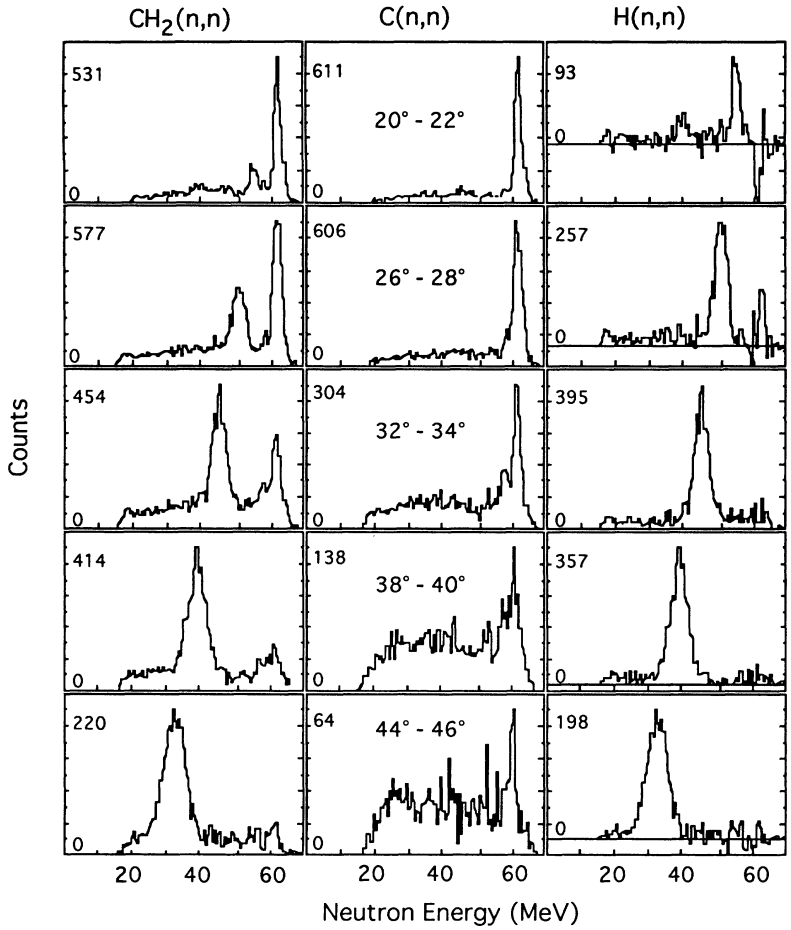

FIG. 2. Extracted 65 MeV neutron energy spectra for CH_2 and C targets and subtracted spectra yielding H spectra.

ing macroscopic optical model parameter sets obtained mainly from fits to proton scattering data. Where necessary, the parameters of a model are extrapolated up or down in energy following the energy dependence given.

The C angular distributions are compared with calculations using the OMP's of Watson, Singh, and Segel [13] and Comfort and Karp [15]. These potentials have been obtained by fitting proton elastic and analyzing power data for light nuclei ($7 \leq A \leq 16$) for energies between 10 and 50 MeV (Ref. [13]) and for C up to 185 MeV (Ref. [15]). The calculated neutron angular distributions with these potentials give fair fits to the data, with all of them reproducing the shape of the angular distribution in the entire angular range of the measurements.

The measured neutron elastic differential cross sections from Si, Ca, Fe, Sn, and Pb were compared with calculations using the global "best fit" neutron-nucleus optical model parameters of Becchetti-Greenlees [14], based on an extensive set of proton data below 50 MeV and neutron data below 24 MeV. This potential fits very well the Si angular distributions but the agreement with the data deteriorates as function of increasing A value. The source of this problem could be (1) in the symmetry potential which was obtained only from proton data above 30 MeV, or (2) in the $A^{1/3}$ dependence for all the radius parameters of the potentials, or (3) in the absorption potential, or (4) in the need of coupled channel calculations when strong collective effects are present. However, in order to validate any one of the above assumptions one would have to carry out an extended set of calculations.

The potential (parameter set B) of Patterson, Doering, and Galonsky [14], which is based on that of Becchetti-Greenlees (BG) with the isospin term determined from (p,n) measurements, does not give as good a fit for ^{28}Si. As in the BG case, these potentials were derived from data below 50 MeV, and mostly for $A \geq 40$ MeV.

The Schwandt *et al.* global OMP [16] obtained from fits to the elastic scattering data of 80–180 MeV polarized protons gives a good representation of the present measurements with the exception of the Pb data for angles below 15°. This potential also gives a good fit to the Si data (not shown but very close to that of Becchetti-Greenlees). The Schutt *et al.* [17] OMP, which was obtained by fitting exclusively neutron scattering ($13.5 \leq E_n \leq 40$ MeV) and total cross section ($2 \leq E_n \leq 250$ MeV) data from ^{108}Pb, fits the measurements reasonably well only up to 18°.

Microscopic OMP's

The comparisons of the measured angular distributions with the calculations using the Jeukene-Lejeune-Mahaux [7] (JLM) and Yamaguchi-Nagata-Matsuda [8] (YNM) microscopic OMP's are shown in Fig. 4.

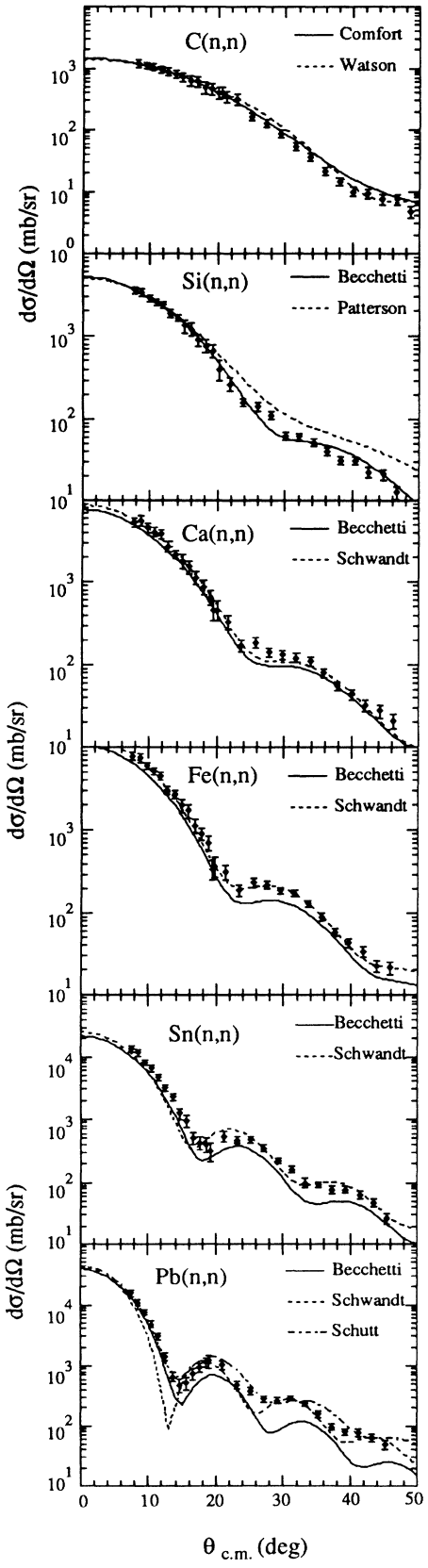

FIG. 3. 65 MeV (n,n) cross sections for natural C, Si, Ca, Fe, Sn, and Pb compared to predictions of several optical model potentials.

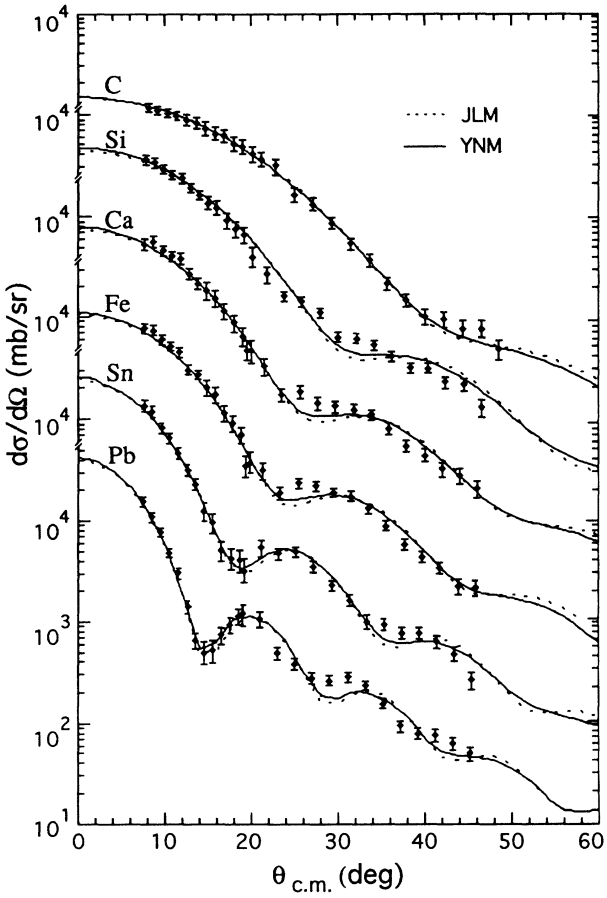

FIG. 4. Fits to the elastic data obtained from the JLM and YNM microscopic optical model potentials for (n,n) scattering at 65 MeV.

These microscopic OMP's are folding potentials of the type

$$U(r,E) = \int t(r,r')\rho(r')dr', \tag{1}$$

where $t(r,r')$ is a complex effective interaction, spin and isospin dependent, which is a function of energy and the nuclear density $\rho(r)$:

$$t(r,r') = t[E,\rho(r'),r,r']. \tag{2}$$

Most of the physics contained in the microscopic OMP's is in the effective interaction and the nuclear density. The main differences between these potentials result from the choice of the effective interaction and in the approximations done in going from infinite nuclear matter to finite nuclei.

The *JLM potential* calculates the potential in infinite nuclear matter from the Reid's hard-core nucleon-nucleon interaction [23] using the Brueckner-Hartree-Fock (BHF) approximation. The potential for the finite nucleus was obtained using an improved [9] local density approximation (LDA), where the effective interaction between the projectile and the target is calculated using the "mid-

point LDA" [the density at which Eqs. (1) and (2) are calculated is evaluated at the position corresponding to the average value of the projectile and target radii $(r + r')/2$]. The JLM potential only includes the central part (real, imaginary, and Coulomb potentials) of the OMP. The spin-orbit (SO) potential is calculated in a folding model [Eq. (1)] using the M3Y interaction (energy and density independent) with Elliot oscillator G-matrix elements as given by Bertsch *et al.* [24].

The *YNM potential* calculates the OMP in infinite nuclear matter from the Hamada-Johnston nucleon-nucleon interaction [25] using the BHF approximation. Only the real part of the SO potential is calculated in addition to the central potential. Calculations of the neutron and proton analyzing power using the YNM spin-orbit interaction (real, energy and density dependent) compare well [12] with the results obtained with the M3Y interaction.

The nuclear density for the neutrons was assumed to be proportional (N/Z) to the proton density. Point-proton densities were obtained by deconvoluting the electron charge density obtained from electron scattering measurements [26]. For the ^{208}Pb(n,n) angular distributions, the proton density used in this calculation was taken from the measurements of Hoffman *et al.* [27], with a neutron skin of 0.14 fm.

The calculations of the elastic scattering and analyzing power angular distributions are done by inserting the microscopic central (real and imaginary) and SO (real only) potentials into a spherical optical model code. The comparison with the data proceeds by a least-square adjustment of three normalizing parameters, λ_V, λ_W, and λ_{SO}, respectively:

$$U = \lambda_V V + i\lambda_W W + \lambda_{SO} V_{SO}. \quad (3)$$

A value of 1 for these parameters indicates that no adjustment of the calculated microscopic potentials is required. The λ_{SO} was not adjusted since in the present work only the elastic scattering angular distributions were measured.

The two microscopic OMP's, JLM and YNM, give very close results in the fits to the (n,n) angular distributions at 65 MeV. However, there are differences in the values of the parameters λ_V and λ_W obtained from the fits to the data shown in Fig. 4. The values are listed in Table I for each of the targets. The deviations from unity for the values of λ_V are about $\pm 10\%$ for the JLM potentials with an average value of 0.97. The average value for the YNM potential is 0.90. These results indicate that the real central potential is well described at this energy by these microscopic models, as was also the case at lower energies [9–12]. The values of λ_W for the JLM potential, with the exception of the C value, are also close to unity with an average value of 0.95. The YNM potential overestimates the absorption potential by almost a factor of 2 and the average value of λ_W, without including C, is 0.613. The correction of the W potential for the C target is in both models much larger than that for the heavier nuclei, which is not surprising for this light nucleus.

The values of the volume integrals for the real and imaginary central potential, J_V/A and J_W/A, calculated for the JLM and YMN potentials, together with the respective total elastic and reaction cross sections, are listed in Table II. These values are in reasonably good agreement with those obtained from an extrapolation up to 65 MeV of the energy-dependent functions given by Winfield *et al.* [28] for J_V for ^{12}C, ^{28}Si, and ^{40}Ca, which were obtained from (n,n) scattering up to 40 MeV. For Si and Ca the agreement is better than 5%, while for C it is around 10%.

Winfield *et al.* [28] discussed the charge symmetry breaking (CSB) in the mean nuclear field. This has been suggested by the Nolen-Schiffer or Coulomb anomaly [29], which is that binding energies in mirror nuclei are larger by 5–10 % than the values calculated taking into account the effects of the Coulomb interactions. The anomaly indicates that V_{nn} is stronger than V_{pp}. Negele [30] calculates that the CSB effect would arise from the difference in the single-particle potential felt by a valence neutron and a valence proton (the neutron feels a more attractive potential than the proton, the difference corresponding to a volume integral of $J^{CSB} = -19$ MeV fm^3 for ^{40}Ca). Winfield *et al.* obtained the following expression for CSB:

$$J^{CSB} = 2(J_n - J'_p)/A \ (\text{MeV fm}^3), \quad (4)$$

where J_n and J_p are the neutron and proton volume integrals of the real central potential and J'_p is obtained by correcting J_p for the Coulomb shift ΔE_C, which the authors calculate following the prescription of DeVito *et al.* [3]. They obtained J^{CSB} values for ^{12}C, ^{28}Si, ^{32}S, and ^{40}Ca of 0 ± 24, -30 ± 11, -29 ± 16, and -8 ± 14 MeV fm^3, respectively. The authors state that the Ca result is perhaps the most reliable, since corrections for coupled channel effects are the smallest for this nucleus. Extrapolat-

TABLE I. Values of the normalizing constants used for the real (λ_V) and imaginary (λ_W) central potentials obtained from a best fit to the data for the JLM and YNM microscopic OMP's.

	JLM			YNM		
Target	λ_V	λ_W	χ^2	λ_V	λ_W	χ^2
C	0.928±0.019	0.658±0.049	3.69	0.937±0.015	0.449±0.030	2.44
Si	1.003±0.052	0.986±0.136	19.7	0.941±0.039	0.661±0.078	13.2
Ca	1.086±0.049	0.985±0.097	9.85	0.996±0.036	0.656±0.056	6.60
Fe	1.033±0.045	0.960±0.080	11.1	0.934±0.034	0.617±0.047	7.63
Sn	0.893±0.029	0.899±0.053	9.90	0.805±0.021	0.557±0.028	6.71
Pb	0.903±0.029	0.926±0.056	17.8	0.814±0.024	0.574±0.031	14.3

TABLE II. Values obtained from microscopic OMP's for the real and imaginary volume integrals per nucleon JV_R/A and JW_I/A (MeV fm^3) and the reaction, elastic, and total cross sections, σ_R, σ_E, and $\sigma_{\rm tot}$ (mb/sr). The fractional uncertainties in the J/A values are to first order given by the fractional uncertainties in the λ values quoted in Table I.

	JLM					YNM				
Target	J_V/A	J_W/A	σ_R	σ_E	$\sigma_{\rm tot}$	J_V/A	J_W/A	σ_R	σ_E	$\sigma_{\rm tot}$
C	337.0	102.9	273.4	449.6	723.0	328.9	91.4	255.7	444.9	700.6
Si	302.2	109.7	552.3	899.8	1452.1	298.4	105.8	564.8	915.4	1480.2
Ca	321.8	106.6	725.8	1201.3	1927.1	312.6	102.3	738.0	1226.1	1964.1
Fe	290.7	91.2	851.6	1447.2	2298.8	282.3	88.3	868.5	1472.8	2341.4
Sn	235.3	71.4	1322.6	2132.2	3454.8	231.7	70.9	1356.6	2149.7	3506.3
Pb	235.6	69.9	1977.2	2533.6	4510.8	232.0	69.5	1985.2	2540.4	4525.2

ing the coupled channel corrections to 65 MeV, one finds that they become very small and within uncertainties are even consistent with zero. Thus we have made no correction for these effects in the values quoted below. The authors [28] also discuss core-polarization effects and calculate these for bound protons and neutrons. The effects, if applicable to scattering states,would increase $J^{\rm CSB}$ by 5–9 MeV fm^3, thus making them less negative. We have not made any such corrections in our values.

Taking an average of the values of J_n obtained with the JLM and YNM microscopic potentials (Table II) and using the expressions of J'_p from Ref. [28] extrapolated up to 65 MeV, values of $J^{\rm CSB}$ equal to -57.6 ± 25.4, -6.4 ± 22.1, and -5.2 ± 20.9 MeV fm^3 are obtained for C, Si, and Ca. The uncertainties in $J^{\rm CSB}$ have been estimated assuming that for J_V/A the JLM and YNM model values and uncertainties are independent and averaging these; and estimating the (smaller) uncertainties in J'_p, from the data given in Ref. [28]. The best agreement with the Winfield *et al.* results is for the Ca values, which could result from having derived the energy dependence function for J'_p from (p,p) data including measurements up to 61 MeV, while for the other nuclei the highest energy was only 40 MeV. Furthermore, although the C values show the largest disagreement, Winfield *et al.* note that the value of 0 ± 24 could have been 22 ± 29 MeV fm^3 depending on which (n,n) data they included in the derivation of the $J^{\rm CSB}$ value for this nucleus. Because of the above-quoted uncertainties and the uncertainties in the corrections due to coupling effects and core polarization, it does not seem meaningful to quote an average value for $J^{\rm CSB}$ from the present data.

IV. CONCLUSIONS

The analysis of the neutron scattering from C, Si, Ca, Fe, Sn, and Pb at 65 MeV was done with global phenomenological [13–17] OMP's and with two microscopic OMP's, the JLM [7] and the YNM [8] potentials. The phenomenological potentials, extracted mainly from (p,p) scattering data over a wide range of energies ($E_p \leq 180$ MeV) and (n,n) data up to 40 MeV, reproduce reasonably well some of the present measurements. However none of the potentials were able to reproduce the (n,n) data over the entire range of A values for these measurements. Both microscopic OMP's gave very good fits to all the data with only two parameters, λ_V and λ_W (normalizing constants to the real and imaginary central potential). The average values of λ_V for the JLM and YNM potentials were 0.97 and 0.90, respectively. The values of λ_W (without including C, which has a larger correction) were 0.95 for the JLM and 0.613 for the YNM potential. The values of these normalizing parameters are an indication that the JLM potential gives a very good representation of the central potential in the optical model, while YNM overestimates the absorption potential by almost 40%.

ACKNOWLEDGMENTS

We are pleased to acknowledge the support of the National Science Foundation(Grants No. PHY8722008, 9024794, and 9123301) and of the IBM Corporation. The support and willing assistance of the staff of Crocker Nuclear Laboratory and the Department of Physics are also gratefully appreciated.

[1] R. P. DeVito, Ph.D. dissertation, Michigan State University, 1979.
[2] R. P. DeVito, S. M. Austin, U. E. P. Berg, R. De Leo, and W. A. Sterrenburg, Phys. Rev. C **28**, 2530 (1983).
[3] R. P. DeVito, S. M. Austin, W. Sterrenburg, and U. E. P. Berg, Phys. Rev. Lett. **47**, 628 (1981).
[4] R. W. Finlay, in *Neutron-Nucleus Collisions—A Probe of Nuclear Structure*, edited by J. Rapaport, R. W. Finlay, S. M. Grimes, and F. S. Dietrich, AIP Conf. Proc. No. 124 (AIP, New York, 1984), p. 527.
[5] P. E. G. Hodgson, Rep. Prog. Phys. **47**, 613 (1984); R. P. DeVito [1], p. 1.
[6] F. A. Brieva and J. R. Rook, Nucl. Phys. **A291**, 299 (1977); **A291**, 317 (1977); **A297**, 206 (1978); **A307**, 493 (1978).
[7] J. P. Jeukenne, A. Lejeune, and C. Mahaux, Phys. Rev. C **15**, 10 (1977); **16**, 80 (1977).
[8] N. Yamaguchi, S. Nagata, and J. Matsuda, Prog. Theor. Phys. **70**, 459 (1983); **76**, 1289 (1986).
[9] S. Mellema, R. W. Finlay, and F. S. Dietrich, Phys. Rev.

C **28**, 2267 (1983).
[10] L. F. Hansen, F. S. Dietrich, B. A. Pohl, C. H. Poppe, and C. Wong, Phys. Rev. C **31**, 111 (1985).
[11] N. Olson, B. Trostell, E. Ramstrom, B. Holmqvist, and F. S. Dietrich, Nucl. Phys. **A472**, 237 (1987).
[12] L. F. Hansen, in *Fast Neutron Physics*, Proceedings of the International Symposium, Beijing, 1991, edited by S. Zuxun, T. Hongqing, X. Jincheng, Z. Jingshang (World Scientific, Singapore, 1992), p. 213.
[13] B. A. Watson, P. P. Singh, and R. E. Segel, Phys. Rev. **182**, 977 (1969).
[14] F. D. Becchetti, Jr., and G. W. Greenlees, Phys. Rev. **182**, 1190 (1969); D. M. Patterson, R. R. Doering, and A. Galonsky, Nucl. Phys. **A263**, 261 (1976).
[15] J. R. Comfort and B. C. Karp, Phys. Rev. C **21**, 2162 (1980).
[16] P. Shwandt, H. O. Meter, W. W. Jacobs, A. D. Bacher, S. E. Vigdor, M. D. Kaitcheck, and T. R. Donoghue, Phys. Rev. C **26**, 55 (1982).
[17] R. L. Schutt, R. E. Shamu, P. W. Lisowski, M. S. Moore, and G. L. Morgan, Phys. Lett. B **203**, 22 (1988).
[18] F. P. Brady, T. D. Ford, G. A. Needham, F. L. Romero, C. M. Castaneda, and M. L. Webb, Nucl. Instrum. Methods Phys. Res. Sect. A **228**, 89 (1984).
[19] J. H. Osborne, J. L. Romero, F. P. Brady, E. L. Hjort, W. P. Caskey, J. Kintner, D. R. Mayo, D. S. Sorenson, and J. L. Ullmann, Nucl. Instrum. Methods Phys. Res. Sect. A (to be published).
[20] J. Binstock, Phys. Rev. C **10**, 19 (1974).
[21] R. A. Arndt and B. J. ver West, in *Proceedings of the 9th International Conference on the Few Body Problem,* Eugene, Oregon, edited by M. J. Moravcski (University of Oregon, Eugene, 1980), Vol. 1.
[22] E. L. Hjort, Ph.D. Dissertation, University of California, Davis, 1990.
[23] R. V. Reid, Jr., Ann. Phys. (N.Y.) **50**, 411 (1968).
[24] G. Bertsch, J. Borysowicz, H. McManus, and W. C. Love, Nucl. Phys. **A284**, 399 (1977).
[25] T. Hamada and I. D. Johnston, Nucl. Phys. **34**, 382 (1962).
[26] C. W. Dejager, H. DeVries, and C. DeVries, At. Data Nucl. Data Tables **14**, 479 (1974).
[27] G. W. Hoffmann, *et al.*, Phys. Rev. C **21**, 1488 (1980).
[28] J. S. Winfield, S. M. Austin, R. P. DeVito, U. E. P. Berg, Z. Chen, and W. A. Sterrenberg, Phys. Rev. C **33**, 1 (1986).
[29] J. A. Nolen, Jr. and J. P. Schiffer, Annu. Rev. Nucl. Sci. **19**, 471 (1969).
[30] J. W. Negele, Nucl. Phys. **A165**, 305 (1971).

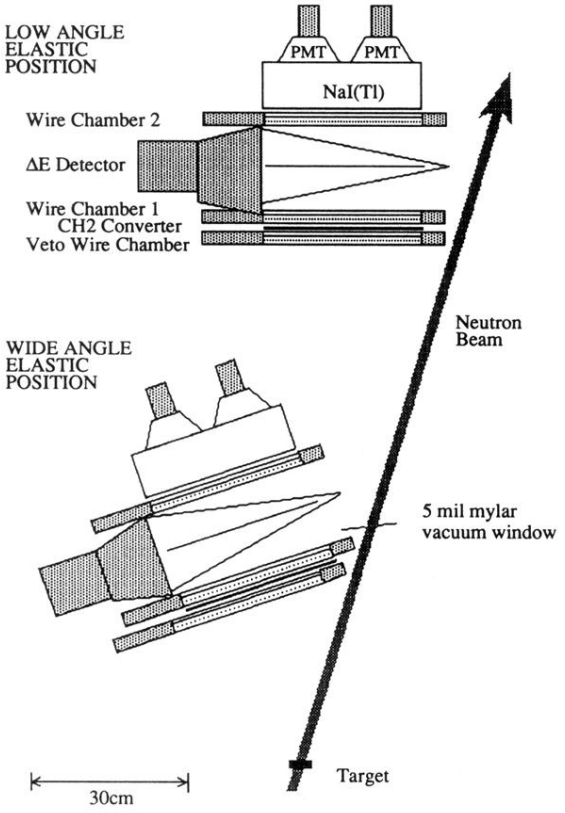

FIG. 1. Scale drawing of the two geometries used for measurement of elastic scattering cross sections. For the low-angle measurements the beam was in vacuum up to the 5 mil Mylar window shown in figure.